e-Polymers **2011**, no. 023

http://www.e-polymers.org

ISSN 1618-7229

Flow induced crystallization of LDPE nanocomposites: A rheological and morphological characterization

Fiorenza Azzurri,[1] Paola Stagnaro,[1] Lucia Conzatti,[1] Dario Cavallo,[2] Luca Repetto,[3] Marco Scatto,[4] Leonardo Andreotti,[4] Serena Coiai[4 5]*

[1*]Institute for Macromolecular Studies, ISMAC-CNR, Via de Marini 6, Genova, Italy; fax: +390106475880; e-mail: azzurri@ge.ismac.cnr.it
[2]Department of Chemistry and Industrial Chemistry, University of Genova - Via Dodecaneso 31, Genova, Italy.
[3]Department of Physics, University of Genova - Via Dodecaneso, 33, Genova, Italy.
[4]Italian Centre for Packaging, CIP, Viale delle Industrie 25, Marghera, Venezia, Italy.
[5]Department of Chemistry and Industrial Chemistry, University of Pisa, Via del Risorgimento 35, Pisa, Italy.

(Received: 08 May, 2009; published: 15 March, 2011)

Abstract: The flow induced crystallization behaviour of a LDPE:PE-g-MA:D72T 90:9:1 nanocomposite has been investigated by in-situ Rheo-SALS technique and data have been compared with those obtained from a reference LDPE:PE-g-MA 90:9 sample. Rheo SALS results, confirming thermal analysis findings, indicate that under mild shear flow fields the organoclay exhibits a negligible nucleating effect. Both nucleation density and, as a consequence, crystallization rate, are not appreciably affected by the application of external flow field for both the examined systems, revealing that no evident synergic effects between the organoclay and the shear flow are present. On the other hand, Rheo SALS analysis indicates that the nanocomposite submitted to flow exhibits a higher level of crystal orientation. TEM morphological analyses support this observation suggesting that the orientation of the nanofiller along the flow direction templates the growth of oriented crystals.

Introduction

In the past years Flow Induced Crystallization (FIC) of macromolecular systems has been largely investigated [1-10] to understand the role of the thermo-mechanical history applied during polymer processing on the final morphology and properties of polymeric materials. A good level of knowledge has been reached and it is well established that application of flow fields before and/or during polymer solidification results in a large increase of nucleation density and, as a consequence, of the overall crystallization rate [1-3,7,10-13].

The application of flow promotes alignment of macromolecular chains along the flow direction, generating oriented nano-ordered aggregates which act as nuclei at the crystallization temperature [4-6,12-20]. FIC studies have been addressed to investigate the role of molecular parameters (composition [21-23], molar mass [24-31], etc) and flow conditions [11-12, 32-34] on the crystallization kinetics of polymers, mainly of polyolefins.

However, FIC behaviour in nanocomposites has received so far little attention; few studies dealing with the flow effects on the crystallization of nano-filled polymeric

materials have been reported [35-42]. In particular, most of them focus on the flow induced crystallization in polypropylene nanocomposites. From time-resolved light scattering experiments, Somwangthanaroj [35] showed that, under flow conditions, intercalated PP/amino-exchanged montmorillonite nanocomposites crystallizes faster than the parent polypropylene. This behaviour was also found by Monasse *et al*. [37]. Recently, Hsiao *et al*. [38] found a similar effect on PP/modified carbon nanofibers. In 2009 Rozanski *et al*.[42] evidenced a strong enhancement of crystallization rate after shearing in exfoliated PP based nanocomposites; however, despite the strong effect on solidification kinetics only a weak orientation of α PP crystals was observed, probably related to the development of a very small population of oriented crystals under shear.

Here we report FIC results obtained, by means of an in-situ Rheo-SALS technique, on LDPE nanocomposite containing 1 wt% of organoclay under low-medium intensity shear flow fields. The effect of shear flow on the morphology has also been investigated by means of TEM.

Results and discussion

Quiescent crystallization

To disclose the coupled role of flow fields and nanoclay on the crystallization kinetics and morphology, a reference sample LDPE:PE-g-MA 90:9 and a nanocomposite LDPE:PE-g-MA:D72T 90:9:1 were investigated.

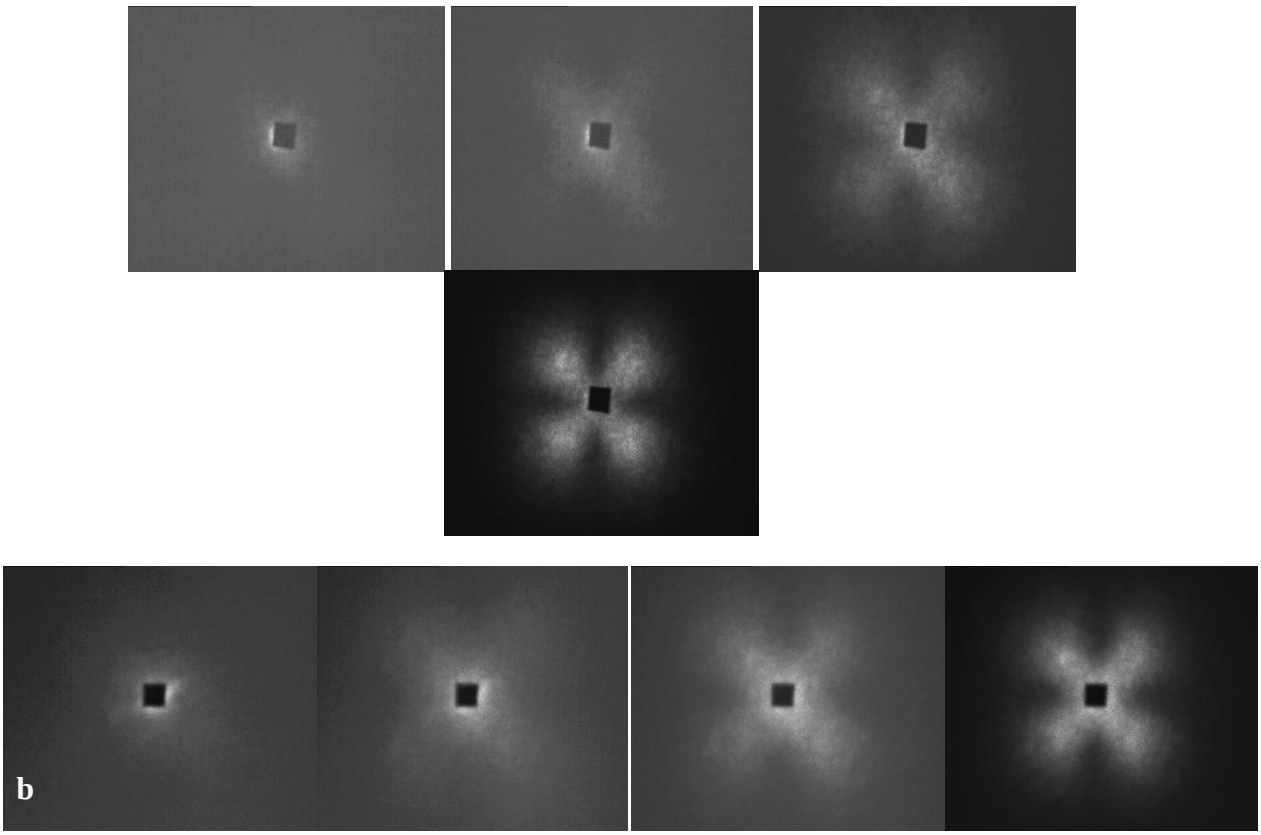

Fig. 1. Scattering patterns for: a) LDPE:PE-g-MA, quiescent crystallization at 99.5, 99, 98 and 95 °C b) LDPE:PE-g-MA:D72T 90:9:1 quiescent crystallization at 101, 100, 99 and 96 °C.

According to the literature [43-48], SALS technique can be successfully adopted to follow the melt crystallization and to appreciate both the characteristic temperatures of the process and the resultant morphology. The adopted experimental protocol is described in the experimental section and the applied flow conditions, carefully selected on the basis of preliminary melt crystallization experiments, are reported in Table 1.

As an example, two sequences of scattering patterns collected during cooling from the molten state for the reference sample LDPE:PE-g-MA 90:9 and for the nanocomposite LDPE:PE-g-MA:D72T 90:9:1 are shown in Figure 1.

Figure 1a, related to the reference sample, evidences that under quiescent conditions the nucleation process starts at 99°C and most of crystallization process takes place in the range between 98 and 95°C. In facts, in the second frame of Figure 1a, the four lobes characteristic of spherulitic morphology appear and the scattering intensity quickly increases on decreasing temperature, thus indicating that crystallization process still continues on cooling.

The analysis of frames recorded on cooling evidences that no changes in pattern intensity can be detectable in the range between 65 an 40°C, suggesting that crystallization is almost completed at these temperatures.

Similarly, Figure 1b, related to the nanocomposite, shows that nucleation begins at 100°C (second pattern) and most of the process takes place between 100 and 96°C.

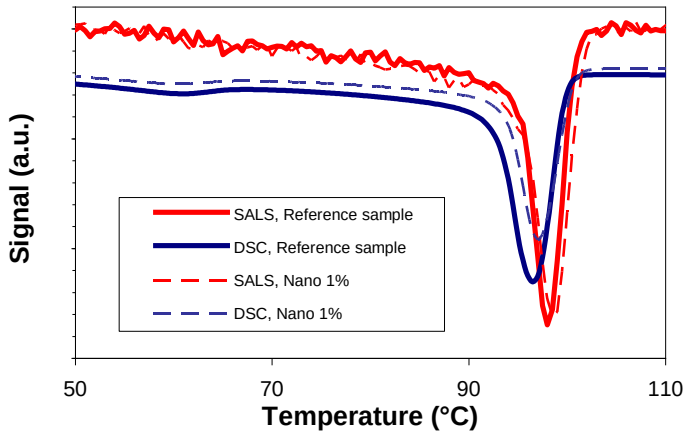

Fig. 2. Crystallization curves for the reference and the nanocomposite samples as derived from DSC and SALS experiments in quiescent conditions.

The temperature derivative of SALS transmitted intensity (dI/dT) is plotted in Figure 2 as a function of temperature. The curves are compared with DSC traces recorded according to the procedure described in the experimental part. SALS crystallization data confirm DSC results: the organoclay does not play any relevant nucleating role, since the reference sample LDPE:PE-g-MA 90:9 and the nanocomposite LDPE:PE-g-MA:D72T 90:9:1 exhibit very close crystallization peak temperatures, T_c, whose difference is within the range of the experimental error.

This result agrees with some literature data referred to LDPE/organo modified nanocomposites [49] and polypropylene/montmorillonite nanocomposites [35,37]. Morawiec *et al.* [49] evidenced by thermal analyses that crystallization kinetics in

LDPE/organo modified systems is not affectd by the presence of organo clay. Similarly, a poor nucleating activity of the clay is usually reported for polypropylene based nanocomposites crystallizing under static conditions.

Flow induced crystallization

In Figure 3 dI/dT as a function of temperature in the shear rates range between 1 and 7 s^{-1} for the reference sample LDPE:PE-g-MA 90:9 is shown. No relevant changes in the crystallization peak temperature on increasing shear rate can be appreciated. Indeed, independently from the adopted shear flow field intensity, crystallization takes place around 98 °C, thus suggesting that the application of low-medium intensity shear flows barely affects the solidification process of LDPE:PE-g-MA 90:9.

This behavior differs from what usually observed for other not compatibilized polyolefins [1, 2, 11-15] for which, as reported in literature, crystallization kinetics dramatically increases on increasing the shear rate.

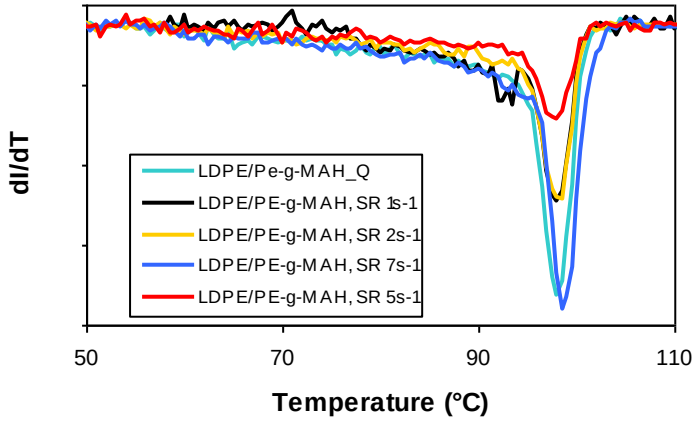

Fig. 3. Crystallization curves for LDPE:PE-g-MA 90:9 from SALS experiments at different shear rate.

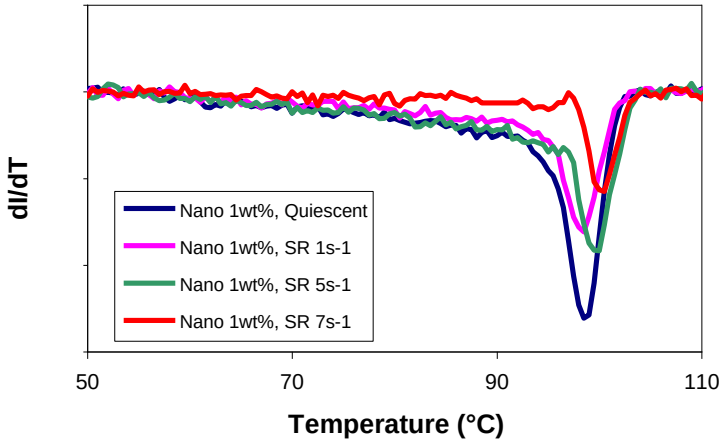

Fig. 4. Crystallization curves for LDPE:PE-g-MA:D72T 90:9:1 from SALS experiments at different shear rate.

On the contrary, from Figure 4, related to the LDPE:PE-g-MA:D72T 90:9:1 nanocomposite, a slightly different situation can be observed. On increasing shear rate, the crystallization peak shifts towards higher temperatures. As an example, when a shear rate of 5 s^{-1} is applied for 3 s at 110 °C, the crystallization peak shifts from 98.5 °C to 100.5 °C.

In Figure 5 a comparison between the crystallization behaviour of the reference and nanocomposite sample is shown. In particular, the nucleation density value, N, as derived from SALS experiments on the basis of equations proposed in the experimental section, is plotted as a function of shear rate. It is evident that, independently from the applied shear rate, both in the LDPE:PE-g-MA 90:9 and in the LDPE:PE-g-MA:D72T 90:9:1, N differs at most by a factors of 2. This indicates that in the investigated system crystallization behaviour under flow is barely affected by the presence of the organoclay.

Nucleation density does not considerably change on increasing shear rate, indicating that the applied flow field is not adequate to produce active nuclei. These results slightly differ with literature data referred to polypropylene nanocomposites [35, 37, 38].

Actually, as shown in Figure 5, in the studied LDPE matrix, even in absence of external flow fields, the number of nuclei is about 5 order of magnitude higher than that usually quantified for other polyolefins crystallized under similar flow conditions [24]. Such high concentration of intrinsic nuclei (*i.e.* those of homogeneous or heterogeneous nature, not generated by flow field) overwhelms that produced by external flow fields. A similar behaviour has been recently reported for flow induced crystallization of polypropylene filled with different nucleating agents [50]. In that work, SAXS-WAXD data demonstrated that only when the concentration of flow induced nuclei is, at least, of the same order of magnitude of those naturally present in the system, the effects of flow can be appreciated.

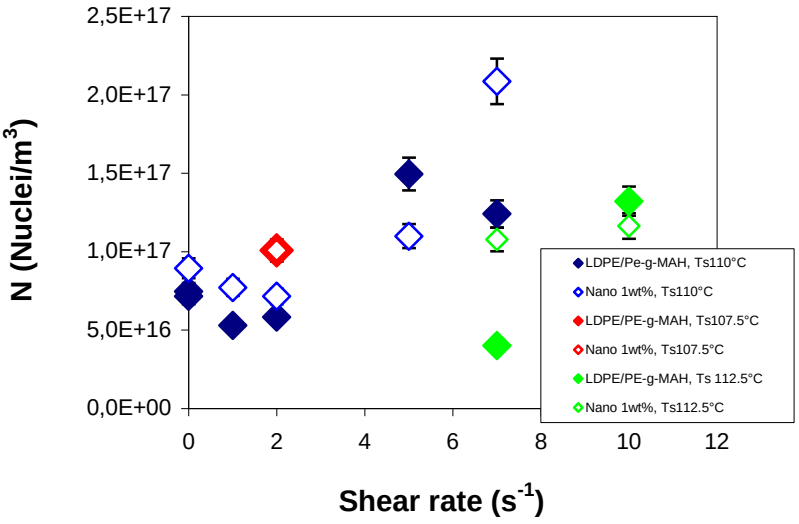

Fig. 5. Nucleation density as evaluated by SALS as function of shear rate for different shearing temperatures.

Moreover, also the relatively low molecular weight of the LDPE matrix can be taken into account to explain the weak effect of flow on crystallization. In facts, as reported

in literature [24-31], when a given shear condition is applied, a low molecular weight should result in a low molecular orientation of the system and, thus, in a reduced enhancement of crystallization rate.

Notwithstanding the weak role of flow fields on the nucleation density of LDPE systems, a high level of orientation can be reached when mild shear flow fields are applied on the nanocomposite sample. In Figure 6a and b the room temperature scattering pattern for the LDPE:PE-g-MA 90:9 and LDPE:PE-g-MA:D72T 90:9:1 nanocomposite sheared at 110 °C at a shear rate of $5s^{-1}$ are shown, respectively.

In Figure 6a the typical Hv four lobes patterns, characteristics of a spherulitic system crystallized under quiescent condition [47], can be observed. In Figure 6b, the stretched four lobes, characteristics of oriented structures are evident. This indicates that, notwithstanding the small effect of nanoclay on nucleation density, the orientation of the nanofiller templates the subsequent growth of oriented crystals.

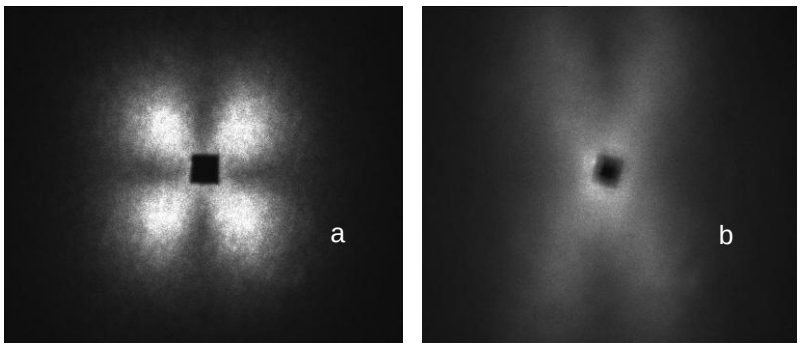

Fig. 6. Final room temperature scattering patterns, in samples sheared at T_s=110 °C, $\dot{\gamma} = 5s^{-1}$ a) not oriented LDPE:PE-g-MA 90:9; b) oriented LDPE:PE-g-MA:D72T 90:9:1.

A quantitative evaluation of the degree of orientation reached under flow can be performed simply by measuring the angle distortion between two lobes, taking into account that the higher is the level of orientation the lower the angle distortion is.

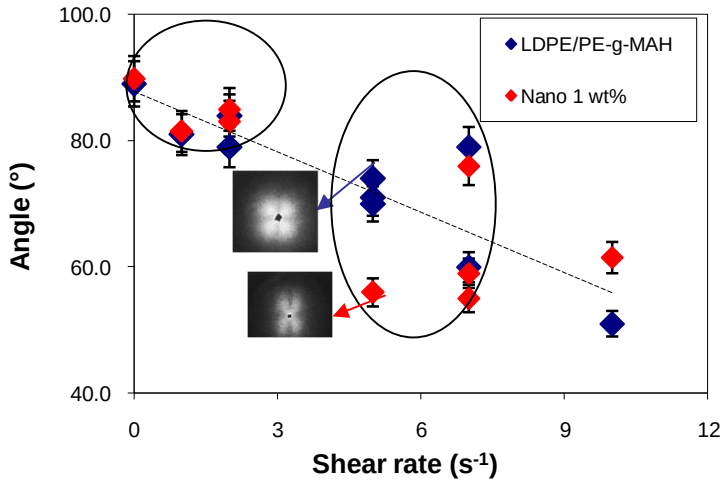

Fig. 7. Orientation, as measured from Hv scattering patterns, as a function of shear rate for reference and nanocomposite samples sheared at different temperatures.

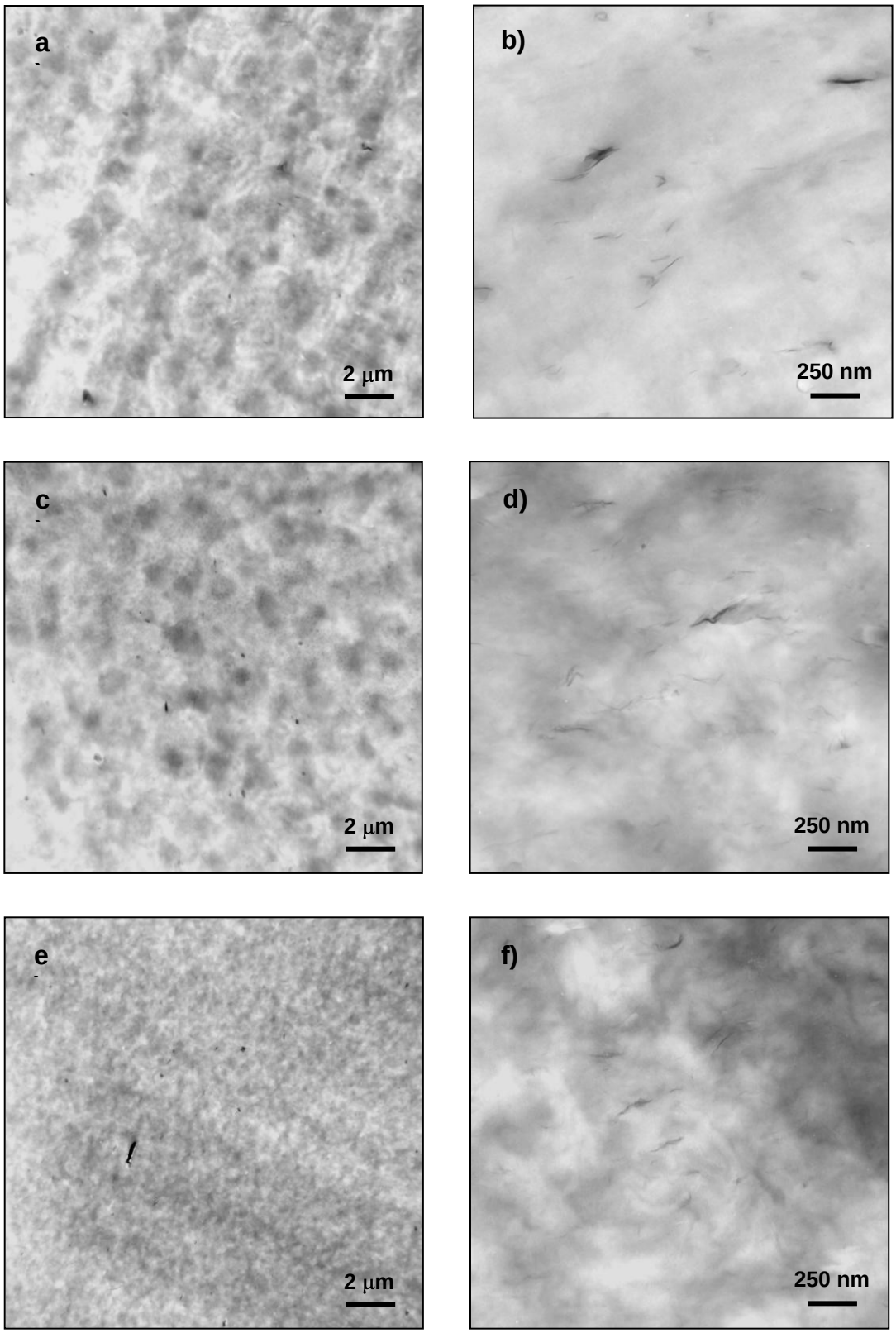

Fig. 8. TEM micrograph of LDPE:PE-g-MA:D72T 90:9:1 film after Rheo-SALS experiments carried out in quiescent conditions (a,b) and under shear: T_s = 110 °C, t_s = 3 s, $\dot{\gamma} = 5s^{-1}$ (c,d), and T_s = 110 °C, t_s = 3 s, $\dot{\gamma} = 7s^{-1}$ (e,f).

In particular, in Figure 7 the angle value between two lobes as a function of shear rate for the reference sample and the nanocomposite system is plotted. As expected the orientation increases on increasing shear rate and the LDPE nanocomposite (red symbols) exhibits a higher level of orientation than the reference system. As proposed by Hsiao *et al* [38], this evidence can be related to the hindrance experienced by polymer chains in their motions, due to the presence of the nanofiller. The resulting delayed chain relaxation is responsible of the slight increase of the amount of orientation. Along this line, the results shown in Figure 7 can be fully justified.

Morphological characterization

A detailed thermal and morphological characterization of LDPE:PE-g-MA 90:9 and LDPE:PE-g-MA:D72T 90:9:1 has been recently reported elsewhere [51]. In particular, the morphological analysis performed by TEM on the LDPE:PE-g-MA:D72T nanocomposite plaques indicates a good dispersion of the organoclay into the polymer matrix, since the sample is mainly composed of exfoliated clay layers, even if intercalated tactoids are sometimes observed.

In order to ascertain the influence of shear flow both on organoclay dispersion and nucleation density (spherulitic crystallization), TEM observations were performed, according to the procedure described in the experimental part, on films obtained after Rheo-SALS experiments carried out both in quiescent conditions and under shear (T_s = 110°C, t_s = 3 s, $\dot{\gamma} = 0,5,7 s^{-1}$).

TEM pictures reported in Figure 8 show that in all the samples single platelets and stacks of layers are present, indicating a mainly exfoliated morphology. The clay particles are evenly dispersed and oriented with respect to shear direction (Figure 8 d,f). However, the application of the shear during cooling does not seem to affect the dispersion and the overall orientation of the clay. It must to be pointed out that the shear rates applied are much lower that those typically applied during polymer processing. On the other hand, as it is clearly seen in Figure 8 a,c,e, the spherulites became smaller, reaching sub-micrometric dimensions, on increasing the shear rate thus confirming the increase in the nucleation density value, N, shown in Figure 5.

Conclusions

Flow induced crystallization of a LDPE:PE-g-MA:D72T 90:9:1 nanocomposites have been studied by in-situ Rheo-SALS experiments and data have been compared with those obtained from a reference LDPE:PE-g-MA 90:9 sample.

Rheo-SALS technique allows acquiring reliable information, comparable with DSC data, on the crystallization behaviour both in quiescent conditions and after the application of low-medium intensity flow fields. Data analysis reveals that the organoclay exhibits a negligible nucleating effect independently from the applied shear rate.

The application of external flow field does not significantly affect the crystallization rate of LDPE:PE-g-MA:D72T 90:9:1 nanocomposite and the crystallization peak temperature is barely affected by the shear rate value. Nucleation density in the modified filled LDPE matrix is very high, much higher than that usually obtained for other polyolefins. N does not change on increasing shear rate, thus suggesting that the application of flow does not modify the crystallization rate of filled LDPE and no

relevant synergism between clay and flow can be appreciated. On the other hand, SALS analysis evidences that the nanocomposite submitted to flow exhibits a higher level of crystal orientation. TEM morphological observations supports Rheo-SALS results and evidence that the organoclay are oriented along the flow direction, thus favouring and templating the subsequent growth of oriented crystals.

Experimental part

LDPE nanocomposites

The LDPE nanocomposite was prepared via direct melt intercalation in a co-rotating twin-screw extruder (THERMO, PolyLab) with a screw diameter of 24 mm and a length-to-diameter ratio (L/D) of 40. The sample was obtained by dilution of a previously prepared masterbatch by mixing the organoclay (Dellite D72T®, Laviosa) with the compatibilizer (PE-g-MA), a maleic anhydride modified polyethylene (UL EP Compoline, Auserpolimeri), the weight proportion between compatibilizer and organoclay being 9:1. In a second step, the masterbatch was melt blended with LDPE (Riblene FL34, Polimeri Europa) to achieve a LDPE:PE-g-MA:D72T 90:9:1 nanocomposite, as reported elsewhere [51].

Thermal Characterization

Thermal characterization was performed with a Mettler Toledo 821^e calorimeter. The sample was held at 180 °C for 5 min and then cooled at 10 °C/min up to 40 °C, in order to appreciate the crystallization peak temperature, T_c, and the crystallization enthalpy associated to the process. Then, in order to define the melting peak temperature, T_m, the specimen was newly heated up to 180 °C, with a heating rate of 10 °C/min.

Rheo-optical characterization

Rheological experiments were performed by means of a plate plate rotational shearing device, Linkam CSS 450, enabling a strict control of temperature (between room temperature and 400 °C, with a control better than 0.5 °C), shear rate and shearing time. As known, in a rotational shearing device the distribution of radial shear rate is expressed by

$$\dot{\gamma} = \frac{\omega R}{d} \qquad (1)$$

where ω is the angular velocity of the rotating plate, R is the radial position along the plate radius and d is the gap between the plates, which can be varied from 10 to 2500 μm. In the present experimental protocol, the gap was fixed at 100 μm.

To perform in-situ Rheo-SALS experiments, according to a well tested experimental procedures [43,44], the Linkam shearing device was mounted on a vertical bench equipped with a He-Ne laser light source (λ = 635 nm) and two polarizers. As shown in Figure 9, according to the Hv configuration [47], these were set at 0 and 90°, respectively.

The Hv scattering patterns were collected on a screen and digitalized with a CCD camera. In particular, the data acquisition and analyses were performed by means of a in house Lab View software.

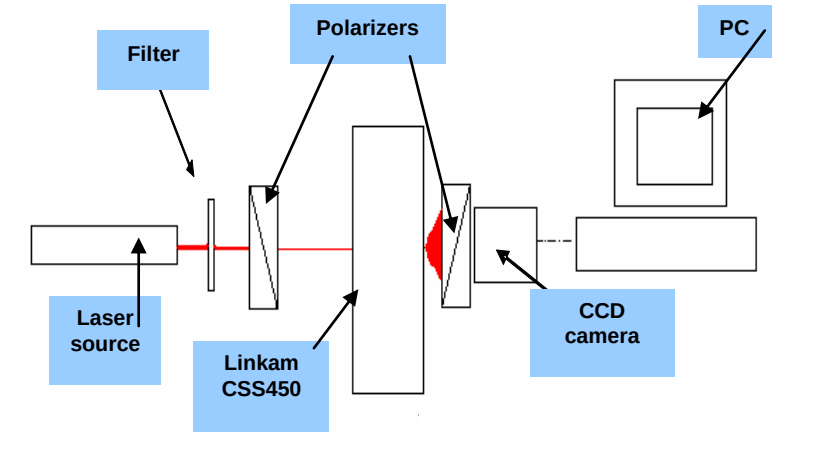

Fig. 9. Equipment for Rheo SALS experiments.

For the Rheo-Optical investigation LDPE:PE-g-MA 90:9 and LDPE:PE-g-MA:D72T 90:9:1 sample films, about 200 μm thick, were prepared from pellets by compression moulding at 170 °C for 5 min in a Carver press, followed by quenching in cold water. Successively, a 25 mm diameter film disk was held between the two quartz plates of the Linkam cell at 170 °C for 5 min, in order to completely erase the memory of previous thermo-mechanical history. Then, the sample was cooled down to 40 °C, at a controlled cooling rate of 10 °C/min.

On cooling, at a suitable shearing temperature, T_s, slightly lower than the observed melting point of the polymer matrix but higher than the crystallization temperature, a short duration step shear was applied. The adopted flow conditions were selected on the basis of quiescent conditions preliminary experiments and have been collected in Table 1

The scattering patterns were recorded, throughout the whole process, at frequency of 1 pattern every 3 s.

As reported in literature, the size of spherulites was deduced by the Hv scattering pattern by averaging the intensity versus the scattering angle over the four lobes. The average radius for spherulites, R, was estimated considering that [48]

$$R = \frac{4.08}{q_{max}} \qquad (2)$$

where q_{max} is the scattering vector corresponding to the maximum Intensity. From R, the nucleation density characteristic of the crystallizing system, N, was quantified by considering that:

$$N / m^3 = \frac{3/4}{\pi (R(m))^3} \qquad (3)$$

Morphological characterization

The morphology of LDPE nanocomposites before and after the application of shear flow fields was investigated by Transmission Electron Microscopy (TEM) by using a Zeiss EM 900 microscope operating at an accelerating voltage of 80 kV. In order to correlate Rheo-SALS information with morphology, TEM observations were performed, after Rheo-SALS experiments, on films crystallized both in quiescent

conditions and after shearing. Taking into account equation 1, narrow stripes were taken along the radius at a given shear rate value and then prepared for TEM by embedding in an epoxy resin and microtoming into ultra-thin sections (about 50 nm thick) with a Leika EM-FCS cryoultramicrotome equipped with a diamond knife (sample temperature: -145 °C; knife temperature: -60 °C). In order to ascertain the flow effects on the developed morphology, TEM observations were performed in parallel to the flow direction.

Tab.1. Shearing conditions adopted for the Rheo-SALS experiments.

Sample	Ts(°C)	ts(s)	
Riblene FL34 quiescent	/	0	0
Riblene FL34	110	3	5
Riblene FL34	110	3	7
LDPE/PE-g-MAH 90/9 quiescent	/	0	0
LDPE:PE-g-MAH 90:9	107.5	3	2
LDPE:PE-g-MAH 90:9	110	3	1
LDPE:PE-g-MAH 90:9	110	3	2
LDPE:PE-g-MAH 90:9	110	3	5
LDPE:PE-g-MAH 90:9	110	3	7
LDPE:PE-g-MAH 90:9	112.5	3	7
LDPE:PE-g-MAH 90:9	112.5	3	10
LDPE/PE-g-MAH/D72T 90:9:1quiescent	/	0	0
LDPE:PE-g-MAH:D72T 90:9:1	107.5	3	2
LDPE:PE-g-MAH:D72T 90:9:1	110	3	1
LDPE:PE-g-MAH:D72T 90:9:1	110	3	2
LDPE:PE-g-MAH:D72T 90:9:1	110	3	5
LDPE:PE-g-MAH:D72T 90:9:1	110	3	7
LDPE:PE-g-MAH:D72T 90:9:1	112.5	3	7
LDPE:PE-g-MAH:D72T 90:9:1	112.5	3	10

References

[1] Eder, G.; Janeschitz-Kriegl, H.; Liedauer, S. *Prog Polym. Sci*. **1990**, *15*, 629.
[2] Eder, G.; Janeschitz-Kriegl, H. *Mater. Sci. Technol*. **1997**, *18*, 269.
[3] Jay, F.; Haudin, J.M.; Monasse, B. *J. Mat. Sci*. **1999**, *34*, 2089.
[4] Kumaraswamy, G.; Issaian, A. M.; Kornfield, J. A. *Macromolecules* **1999**, *32*, 7537.
[5] Somani, R. H.; Hsiao, B. S; Nogales, A.; Srinivas, S.; Tsou, A. H.; Sics, I.; Baltà Calleja, F. J.; Ezquerra, T. *Macromolecules* **2000**, *33*, 9385.
[6] Somani, R. H.; Hsiao, B. S.; Nogales, A.; Fruitwala, H.; Srinivas, S.; Tsou, A. H. *Macromolecules*, **2001**, *34*, 5902.
[7] Koscher, E.; Fulchiron, R. *Polymer* **2002**, *43*, 6931.
[8] Janeschitz-Kriegl, H.; Ratajski, E.; Steldbauer, M. *Rheol. Acta* **2003**, *42*, 355.
[9] Van Meerveld, J.; Peters, G. V. M.; Hutter, M. *Rheol. Acta* **2004**, *43*, 119.
[10] Janeschitz-Kriegl, H. *Macromolecules* **2006**, *39*, 4448.
[11] Alfonso, G. C.; Scardigli, P. *Macromol. Chem. Phys., Macromol. Symp*. **1997**, *118*, 323.
[12] Azzurri, F.; Alfonso, G. C. *Macromolecules* **2005**, *38*, 1723.

[13] Azzurri, F.; Alfonso, G. C. *Macromolecules* ***2008****, 41,* 1377.
[14] Somani, R. H.; Yang, L.; Hsiao, B. S.; Sun, T.; Pogodina, N. V.; Lustiger, A. *Macromolecules* **2005**, *38*, 1244.
[15] Nogales, A.; Hsiao, B. S.; Somani, R. H.; Srinivas, S.; Tsou, A. H.; Baltà-Calleja, F. J.; Ezquerra, T. A. *Polymer* **2001**, *42*, 5247.
[16] Somani, R.H.; Yang, L.; Hsiao, B.S.; Agarwal, P.K.; Fruitwala, H.A.; Tsou, A.H. *Macromolecules* **2002**, *35*, 9096.
[17] Somani, R. H.; Yang, L.; Hsiao, B. S. *Phys. A.* **2002**, *304*, 145.
[18] Li, L.; De Jeu, W. H. *Macromolecules* **2003**, *36*, 4862.
[19] Garcia Gutierrez, M. C.; Alfonso, G. C.; Riekel, C.; Azzurri, F. *Macromolecules* **2004**, *37*, 478.
[20] Ogino, Y.; Fukushima, H. ; Takahashi, N. ; Matsuba, G.; Nishida, K.; Kanaya, T. *Macromolecules* **2006,** *39***,** 7617.
[21] Heeley, H.; Fernyhough, C. M.; Graham, R. S.; Olmsted, P.; Inkson, N. J.; Embery, J.; Groves, D. J.; McLeish, T. C. B.; Morgovan, A. C.; Meneau, F.; Bras, W.; Ryan, A. J. *Macromolecules* **2006**, *39*, 5058.
[22] An, Y.; Holt, J. J.; Mitchell, G. R.; Vaughan, A. S. *Polymer* **2006**, *47*, 5643.
[23] Somani, R. H.; Yang, L.; Hsiao, B. S.; Fruitwala, H. *J. Macromol. Sci . Part B Phys* **2003**, *42*, 515.
[24] Bove, L.; Nobile, M. R. *Macromol. Symp*. **2002**, *185*, 135.
[25] Acierno, S.; Palomba, B.; Winter, H. H.; Grizzuti, N. *Rheol. Acta* **2003**, *42*, 243.
[26] Elmoumni, A.; Gonzalez Ruiz, R.; Coughlin, B.; Winter, H. H. *Macromol. Chem. Phys*. **2005**, *206*, 125.
[27] Somani, R. H.; Yang, L.; Hsiao, B. S. *Polymer* **2006**, *47*, 5657.
[28] Ogino, Y.; Fukushima, H.; Matsuba, G.; Takahashi, N.; Nishida, K.; Kanaya, T. *Polymer* **2006**, *47*, 5669.
[29] Hadinata, C.; Gabriel, C.; Ruellmann, M.; Kao, N.; Laun, H. M. *Rheol. Acta* **2006**, *45*, 539.
[30] Isayev, A.I .; Chan, T. W.; Shimojo, K.; Gmerek, M. *J. Appl. Polym. Sci*. **1995**, *55*, 807.
[31] Chai, C. K.; Dixon, N. M.; Gerrard, D. L.; Reed, W. *Polymer* **1995**, *36*, 661.
[32] Coppola, S.; Balzano, L.; Gioffredi, E.; Maffettone, P. L.; Grizzuti, N. *Polymer* **2004**, *45*, 3249.
[33] Van der Beek, M. H. E.; Peters, G. W. M.; Meijer, H. E. N. *Macromolecules* **2006**, *39*, 1805.
[34] Baert, J; Van Puyvelde, P. *Polymer* **2006**, *47*, 5871.
[35] Somwangthanaroj, A.; Lee, E.C.; Solomon, M.J. *Macromolecules* **2003**, *36*, 2333.
[36] Malwitz, M.; Dundigalla, A.; Ferreiro, V.; Butler, P.D.; Henk, M.; Schmidt, G. *Phys. Chem. Chem. Phys*. **2004**, *6*, 2977.
[37] Nowacki, R.; Monasse, B.; Piorkowska, E.; Galeski, A.; Haudin, J.M. *Polymer* **2004**, *45*, 4877.
[38] Kelarakis, A.; Yoon, K.; Somani, R.H.; Chen, X.; Hsiao, B.S.; Chu, B. *J. Macromol. Sci. Part B* **2006**, *45*, 247.
[39] Garcia Gutierrez, M.C.; Nogales, A.; Rueda, D.; Domingo, C.; Garcia-Ramos, J.V.; Broza, G.; Roslaniec, Z.; Schulte, K.; Dvies, R.J.; Ezquerra, T. *Polymer* **2006**, *47*, 341.
[40] Lee, S.H.; Youn, *J.R. Adv. Comp. Mat*. **2008**, *17*, 191.
[41] Mago, G.; Fisher, F.T.; Kalyon, D. M. *Macromolecules* **2008**, *41*, 8103.

[42] Rozanski, A; Monasse, B.; Szkudlarek, E.; Piorkowska, E.; Galeski, A.; Haudin, J.M. E. Polym. J. **2009**, *45*, 88, 101.
[43] Chai, C.K.; Auzoux, Q.; Randriantoandro, H.; Navard, P.; Haudin, J.M. *Polymer* **2003**, *44*, 773.
[44] Fukushima, H.; Ogino, Y., Matsuba, G.; Nishida, K.; Kanaya, T. *Polymer* **2005**, *46*, 1878.
[45] Stein, R.S.; Wilson, P.R. *J. Appl. Phys*. **1962**, *33*, 1914.
[46] Stein, R.S.; Hotta, T. *J. Appl. Phys*. **1964**, *35*, 2237.
[47] Stein, R.S.; Cronauer, J.; Zachmann, H.G. *J. Mol. Str*. **1996**, *383*, 19.
[48] Okada, T.; Saito, H.; Inoue, T. *Macromolecules*, **1992,** *25*, 1908.
[49] Morawiec, J.; Pawlak, A.; Slouf, M.; Galeski, A.; Piorkowska, E.; Krasnikova, N. E. Polym. J. **2005**, *41*, 1115.
[50] Byelov, D.; Panine, P.; Remerie, K.; Biemond, E.; Alfonso, G.C.; De Jeu, W.H.; *Polymer* **2008**, *49*, 3076.
[51] Coiai, S.; Scatto, M.; Bertoldo, M.; Conzatti, L.; Andreotti, L.; Sterner, M.; Passaglia, E.; Costa G.; Ciardelli, F. *e-Polymers*, **2009**, no 050.